






## Hydrothermal synthesis, structural investigation, and magnetic properties of 2-D layered lanthanide (Ln = Pr, Eu, Gd, Tb, and Er) coordination polymers possessing infinite 1-D nanosized cavities

Shahzad Sharif, Onur Şahin, Bushra Khan & Islam Ullah Khan


To cite this article: Shahzad Sharif, Onur Şahin, Bushra Khan & Islam Ullah Khan (2015) Hydrothermal synthesis, structural investigation, and magnetic properties of 2-D layered lanthanide (Ln = Pr, Eu, Gd, Tb, and Er) coordination polymers possessing infinite 1-D nanosized cavities, Journal of Coordination Chemistry, 68:15, 2725-2738, DOI: [10.1080/00958972.2015.1056739](https://doi.org/10.1080/00958972.2015.1056739)


To link to this article: <http://dx.doi.org/10.1080/00958972.2015.1056739>

 View supplementary material 

 Accepted author version posted online: 05 Jun 2015.  
Published online: 10 Jul 2015.

 Submit your article to this journal 

 Article views: 83

 View related articles 

 View Crossmark data 

## Hydrothermal synthesis, structural investigation, and magnetic properties of 2-D layered lanthanide (Ln = Pr, Eu, Gd, Tb, and Er) coordination polymers possessing infinite 1-D nanosized cavities

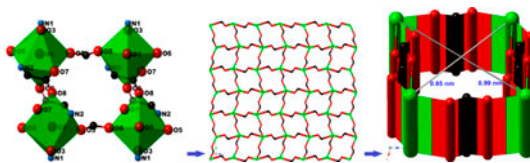
SHAHZAD SHARIF\*†, ONUR ŞAHİN‡, BUSHRA KHAN† and ISLAM ULLAH KHAN§

†Department of Chemistry, Lahore College for Women University, Lahore, Pakistan

‡Scientific and Technological Research Application and Research Center, Sinop University, Sinop, Turkey

§Materials Chemistry Laboratory, Department of Chemistry, GC University, Lahore, Pakistan

(Received 29 August 2014; accepted 26 March 2015)



Tetrahedral SBUs to construct 2D net having nanosized cavities.

Five 2-D Ln(III) coordination polymers,  $[\text{Ln}(\text{PDA})(\text{PDAH})]_n$  (PDA = 2,6-pyridinedicarboxylate), have been obtained under mild hydrothermal condition. In each coordination polymer, PDA is tetradentate and pentadentate, while lanthanides have coordination number eight to generate trigonal prismatic, triangular face biccapped  $\text{LnO}_6\text{N}_2$  geometry having 9 triangular and 2 square faces. Two different types of bridging oxygens are responsible to grow the 2-D coordination polymers providing open channels possessing infinite 1-D nanosized cavities. Adjacent 2-D chains are further extended to a 3-D hydrogen-bonded layered network through intermolecular  $\pi$ - $\pi$  interactions and  $\text{C-H}\cdots\text{O}$  hydrogen bonds. Four lanthanides are arranged roughly at the vertices of a square and bridged by eight carboxylates leading to the overall tetrahedral shape of the secondary building units. The abnormal behavior of lanthanide contraction for the atomic radii of europium can be attributed to overlapping of electron clouds. The overall magnetic behavior is typical for the presence of anti-ferromagnetic exchange coupling interactions. Thermal decomposition analysis reveals that the coordination polymers have significant thermal stability. The coordination polymers are further characterized using elemental analysis and FT-IR spectroscopy.

**Keywords:** Pyridine-2,6-dicarboxylic acid; Lanthanide; Sodium azide; 2D coordination polymer; Nanosized

\*Corresponding author. Emails: [msharif@gcu.edu.pk](mailto:msharif@gcu.edu.pk), [msharifcwu@gmail.com](mailto:msharifcwu@gmail.com)

## 1. Introduction

Construction of lanthanide organic frameworks (LOF) with oxygen donor ligands is an area of intense research owing to fascinating structures and potential applications in storage, catalysis, separation, and magnetic materials [1–5]. Coordination modes of multidentate oxygen donor ligands and flexible coordination geometry as well as variable coordination numbers of lanthanides are responsible to generate various LOFs [6–10]. It is, however, difficult to predict the resultant LOF structure as there are parameters involved such as coordination geometry of ligand, solvent polarity, pH of solution [11–15], metal to ligand ratio [11–14, 16–18], reaction time, and temperature [11–14, 16–18]. Among these factors, pH plays a major role for construction of coordination polymers. PDAH<sub>2</sub> owing to multidentate coordination sites can be partially or completely deprotonated to generate PDAH<sup>−</sup> and PDA<sup>2−</sup> anions. Hence, carefully controlling the pH allows PDAH<sub>2</sub> to display various pH-dependent coordination modes and possibly form higher dimensional polymers [19(a) and (b)].

We have focused on studies to explore coordination behavior of multidentate oxygen donor ligands [19(c)–(g)]. A review of the literature reveals that most LOFs are synthesized by keeping the reaction mixture under autogenous pressure for more than 3 days via hydrothermal methods [15, 20]. Previously, Li *et al.* [20(d)] and Fernandes *et al.* [20(h)] reported isostructural holmium and dysprosium LOFs by keeping the reaction mixture at a lower pH under hydrothermal conditions for 3 days. Herein, we have attempted to develop a method to obtain LOF under mild hydrothermal conditions using sodium azide to control the pH of the reaction mixture and ultimately reduce the reaction time. At this stage, we are unable to suggest a detailed mechanism of rapid coordination of ligand with metals; However, it may be ascribed to deprotonation of ligand in the presence of sodium hydroxide, generated *in situ* by reaction of sodium azide and water [15]. Given that the geometries of secondary building units (SBUs) of lanthanide-metal carboxylate clusters play an important role in constructing a LOF [21], we observe a tetrahedral SBU responsible for the formation of the 2-D LOF. PDA adopts two kinds of coordination, including a full coordination mode as shown in figure 1, while Ln(III) lies at the core of a surrounding of eight donors (figure 2). The LOFs were also characterized by FT-IR, elemental, and thermogravimetric analyses.

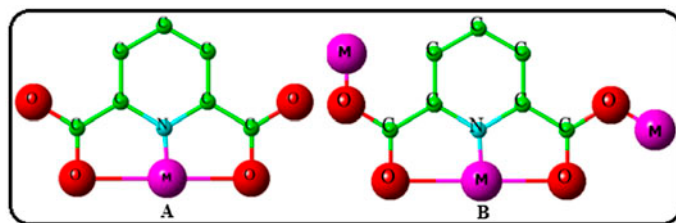


Figure 1. Coordination modes of PDA for 1–5.

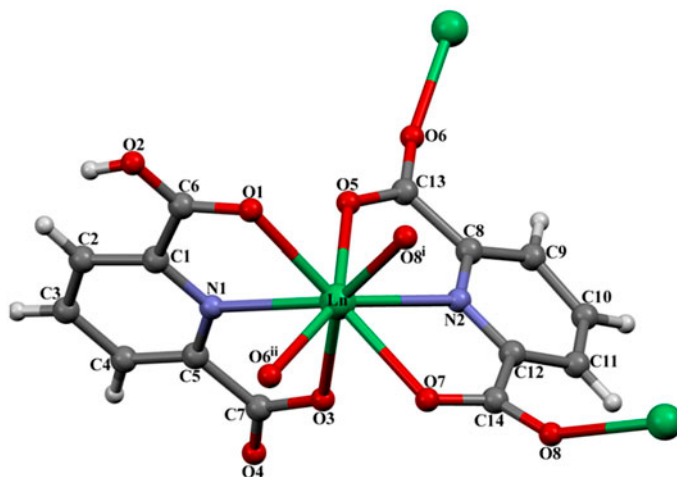


Figure 2. The molecular structure of coordination polymers: Erbium Er(III), Gadolinium Gd(III), Terbium Tb(III), Europium Eu(III), and Praseodymium Pr(III) in 1–5, respectively, showing the atom numbering scheme (symmetry codes as in table S1 [see online supplemental material at <http://dx.doi.org/10.1080/00958972.2015.1056739>]).

## 2. Experimental

### 2.1. Materials and measurements

All reagents were purchased commercially and used without purification. Hydrothermal synthesis were performed using a 23 mL capacity Teflon-lined stainless steel autoclave (Parr Instruments, USA) and temperature programmed oven. Single-crystal data were collected using a Nonius Kappa-CCD Diffractometer, Netherlands, equipped with Oxford Cryosystem, a data collection: COLLECT [22] at 150 K (graphite monochromated Mo-K $\alpha$  radiation,  $\lambda = 0.71073$  Å), cell refinement: DENZO/SCALEPACK, data reduction: DENZO/SCALEPACK [23]. The structures were solved by direct methods with SHELXS and CRYSTALS and the resulting atomic models were developed and refined against  $|F|^2$  with SHELXL and CRYSTALS [24, 25]; the “observed data” threshold for calculating the  $R(F)$  residuals was set as  $I > 2\sigma(I)$ . The C- and N-bound hydrogens were placed in idealized locations (C–H = 0.96–0.97 Å, N–H = 0.86 Å) and refined as riding. The O-bound hydrogens were located in difference maps and refined as riding in as-found relative locations. All non-hydrogen atoms were refined with anisotropic parameters. The structural models were analyzed and validated with PLATON [26], and full refinement details are given in the deposited CIF. Program used for molecular graphics was Mercury [27]; software used to prepare material for publication was WinGX [28]. Supramolecular and polyhedral analyses were performed and the diagrams were prepared with the aid of PLATON and CrystalMaker<sup>®</sup> [26, 29]. Thermal analyses (25–1000 °C) were recorded under continuous nitrogen flow with a ramp rate of 10 °C min<sup>-1</sup> using a SDT Q600 instrument (TA Instruments, USA). Elemental analyses of N, C, and H were performed on Elemental Analyzer, Vario Micro Cube, Elementar, Germany. FT-IR spectra were recorded on a Bruker Tensor 27 FT-IR spectrometer with Diamond-ATR module from 4000 to 400 cm<sup>-1</sup>. All the isolated coordination polymers are stable in air and almost insoluble in water and common organic solvents [30, 31]. The temperature dependence of the magnetic susceptibilities was recorded

at an applied magnetic field of 1000 Oe from 5 to 300 K using a Superconducting Quantum Interference Device (SQUID-MPMS-5, USA). The results are shown as plots of  $\chi_m$ ,  $\chi_m^{-1}$ , and  $\chi_m T$  versus  $T$  ( $\chi_m$  molar magnetic susceptibility) using Origin software [32]. The effective magnetic moments,  $\mu_{\text{eff}}$ , were calculated by applying the relation  $\mu_{\text{eff}} = 2.828 (\chi_m T)^{1/2}$  in Bohr magnetons ( $\mu_B$ ) [33].

## 2.2. Synthesis

**2.2.1. Synthesis of  $C_{14}H_7ErN_2O_8$  (1).** A mixture of PDAH<sub>2</sub> (84 mg, 0.5 mmol), sodium azide (33 mg, 0.5 mmol), erbium chloride hexahydrate (ErCl<sub>3</sub>·6H<sub>2</sub>O; 90 mg, 0.25 mmol), and 7 mL distilled water was sealed in a 23-mL Teflon-lined stainless steel autoclave and heated to 170 °C at a rate of 60 °C h<sup>-1</sup> for 24 h and cooled to room temperature at a rate of 30 °C h<sup>-1</sup>. Pink cube-like crystals were directly filtered from the resultant mixture, washed with plenty of water, and dried at ambient temperature. Analysis (%) Calcd for C<sub>14</sub>H<sub>7</sub>N<sub>2</sub>O<sub>8</sub>Er (498.48): N, 5.62; C, 33.70; H, 1.40. Found: N, 5.51; C, 33.78; H, 1.52. Yield *ca.* 60%. Warning: metal azides are potentially explosive; we found no problems in this work, but only small amounts should be used by taking appropriate safety precautions.

**2.2.2. Synthesis of  $C_{14}H_7GdN_2O_8$  (2).** The procedure was the same as that in **1** except that ErCl<sub>3</sub>·6H<sub>2</sub>O was replaced by GdCl<sub>3</sub>·6H<sub>2</sub>O. Off-white, cube-like crystals were directly filtered from the resultant mixture, washed with plenty of water, and dried at ambient temperature. Analysis (%) Calcd for C<sub>14</sub>H<sub>7</sub>N<sub>2</sub>O<sub>8</sub>Gd (488.47): N, 5.73; C, 34.39; H, 1.43. Found: N, 5.61; C, 34.35; H, 1.48. Yield *ca.* 62%.

**2.2.3. Synthesis of  $C_{14}H_7TbN_2O_8$  (3).** The procedure was the same as that in **1** except that ErCl<sub>3</sub>·6H<sub>2</sub>O was replaced by TbCl<sub>3</sub>·6H<sub>2</sub>O. Off-white, cube-like crystals were directly filtered from the resultant mixture, washed with plenty of water, and dried at ambient temperature. Analysis (%) Calcd for C<sub>14</sub>H<sub>7</sub>N<sub>2</sub>O<sub>8</sub>Tb (490.14): N, 5.71; C, 34.28; H, 1.43. Found: N, 5.48; C, 34.18; H, 1.52. Yield *ca.* 57%.

**2.2.4. Synthesis of  $C_{14}H_7EuN_2O_8$  (4).** The procedure was the same as that in **1** except that ErCl<sub>3</sub>·6H<sub>2</sub>O was replaced by EuCl<sub>3</sub>·6H<sub>2</sub>O. Off-white, cube-like crystals were directly filtered from the resultant mixture, washed with plenty of water, and dried at ambient temperature. Analysis (%) Calcd for C<sub>14</sub>H<sub>7</sub>N<sub>2</sub>O<sub>8</sub>Eu (483.18): N, 5.79; C, 34.77; H, 1.45. Found: N, 5.81; C, 34.81; H, 1.50. Yield *ca.* 58%.

**2.2.5. Synthesis of  $C_{14}H_7PrN_2O_8$  (5).** The procedure was the same as that in **1** except that ErCl<sub>3</sub>·6H<sub>2</sub>O was replaced by PrCl<sub>3</sub>·6H<sub>2</sub>O. Green cube-like crystals were directly filtered from the resultant mixture, washed with plenty of water, and dried at ambient temperature. Analysis (%) Calcd for C<sub>14</sub>H<sub>7</sub>N<sub>2</sub>O<sub>8</sub>Pr (472.13): N, 5.93; C, 35.58; H, 1.48. Found: N, 5.79; C, 35.76; H, 1.53. Yield *ca.* 60%.

Table 1. Crystal data and structure refinement parameters for 1–5.

	1	2	3	4	5
Empirical formula	C <sub>14</sub> H <sub>7</sub> ErN <sub>2</sub> O <sub>8</sub>	C <sub>14</sub> H <sub>7</sub> GdN <sub>2</sub> O <sub>8</sub>	C <sub>14</sub> H <sub>7</sub> TbN <sub>2</sub> O <sub>8</sub>	C <sub>14</sub> H <sub>7</sub> EuN <sub>2</sub> O <sub>8</sub>	C <sub>14</sub> H <sub>7</sub> PrN <sub>2</sub> O <sub>8</sub>
Formula weight	498.48	488.47	490.14	483.18	472.13
Temperature (K)	150				
Wavelength (Å)	0.71073 Mo-K $\alpha$				
Crystal system	Monoclinic	Monoclinic	Monoclinic	Monoclinic	Monoclinic
Space group	<i>P</i> 2 <sub>1</sub> / <i>c</i>	<i>P</i> 2 <sub>1</sub> / <i>c</i>	<i>P</i> 2 <sub>1</sub> / <i>c</i>	<i>P</i> 2 <sub>1</sub> / <i>c</i>	<i>P</i> 2 <sub>1</sub> / <i>c</i>
<i>a</i> (Å)	12.1178(4)	12.2565(3)	12.1940(2)	12.2523(3)	12.2391(4)
<i>b</i> (Å)	8.3510(3)	8.3830(2)	8.3826(1)	8.3957(2)	8.3939(3)
<i>c</i> (Å)	13.3959(5)	13.5429(4)	13.4807(2)	13.5562(3)	13.5328(5)
$\beta$ (°)	102.264(2)	102.421(1)	102.398(1)	102.450(1)	102.469(2)
<i>V</i> (Å <sup>3</sup> )	1324.67(8)	1358.91(6)	1345.83(3)	1361.69(6)	1357.48(8)
<i>Z</i>	4	4	4	4	4
Absorption coefficient (mm <sup>-1</sup> )	6.39	4.93	5.31	4.66	3.64
<i>D</i> <sub>calcd</sub> (Mg m <sup>-3</sup> )	2.499	2.388	2.419	2.357	2.310
Theta range for data collection (°)	5.1–26.0	4.1–26.0	4.1–26.0	5.1–26.0	5.1–26.0
Measured reflections	4748	2662	2639	2661	2657
Independent reflections, <i>R</i> <sub>int</sub>	2571, 0.026	2662, 0.001	2639, 0.001	2661, 0.001	2657, 0.001
Observed reflections [ <i>I</i> > 2 $\sigma$ ( <i>I</i> )]	2315	2193	2506	2288	2114
Absorption correction	Multi-scan DENZO/SCALEPACK [23]				
Refinement method	Full-matrix least-squares on <i>F</i> <sup>2</sup>				
Final <i>R</i> indices (all data)	<i>R</i> 1 = 0.025 <i>wR</i> 2 = 0.059	<i>R</i> 1 = 0.035 <i>wR</i> 2 = 0.083	<i>R</i> 1 = 0.018 <i>wR</i> 2 = 0.045	<i>R</i> 1 = 0.026 <i>wR</i> 2 = 0.059	<i>R</i> 1 = 0.038 <i>wR</i> 2 = 0.093
Goodness-of-fit on <i>F</i> <sup>2</sup>	1.10	1.05	1.10	1.08	1.06
$\Delta\rho_{\max}$ (e Å <sup>-3</sup> )	0.76	1.00	0.67	1.09	2.42
$\Delta\rho_{\min}$ (e Å <sup>-3</sup> )	-1.15	-1.45	-0.99	-0.95	-1.44

### 3. Results and discussion

#### 3.1. Description of structures 1–5

The crystallographic analyses reveal that 1–5 are similar. Complexes 1–5 all crystallize in the monoclinic space group *P*2<sub>1</sub>/*c*. Details of crystal structures are given in table 1. Coordinated bond lengths and angles are reported in table S1 together with other relevant geometrical data.

The molecular structures of 1–5 are depicted in figure 2 with the atom numbering scheme. The asymmetric units of 1–5 contain one Ln(III) (Ln = Er in 1, Ln = Gd in 2, Ln = Tb in 3, Ln = Eu in 4, and Ln = Pr in 5), one PDA<sup>2-</sup>, and one PDAH<sup>-</sup>. Each Ln(III) is eight-coordinate in a conventional O,N,O'-tridentate fashion containing two nitrogens (N1 and N2) from two different pyridine rings, four oxygens (O1, O3, O5, and O7) from two different PDA ligands and two oxygens (O6<sup>ii</sup> and O8<sup>i</sup>) from two different bridging carboxylate groups (figure 2) to generate trigonal prismatic, triangular face bicapped LnO<sub>6</sub>N<sub>2</sub> coordination geometry having 9 triangular and 2 square faces O8/O7/O3/N1 and O8/O6/O5/N1 (figure 3). There are two types of coordination polymers for 1–5, with the first of these coordination polymers running parallel to the [0 0 1] direction. Ln(III) ions are coordinated by O6 of carboxylic groups from symmetrically related PDA anions to generate an infinite 1-D (Ln–OCO–Ln–OCO–Ln)<sub>∞</sub> wavelike chain motif formed through the carboxylate bridges (OCO) [figure 4(a)]. In the second coordination polymer running parallel to the [0 1 0] direction, the Ln(III) ions are coordinated by O8 of carboxylic groups from symmetrically related PDA anions to generate infinite 1-D (Ln–OCO–Ln–OCO–Ln)<sub>∞</sub> ropes

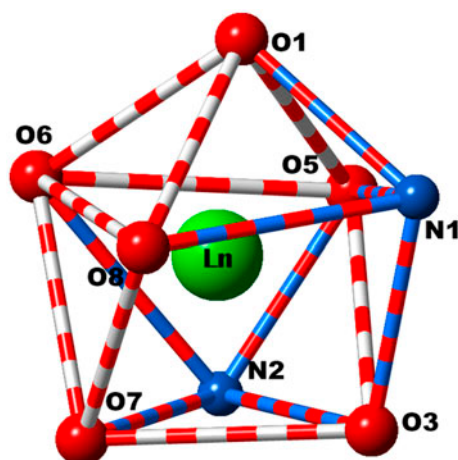


Figure 3. Coordination geometry around the Er(III), Gd(III), Tb(III), Eu(III), and Pr(III) in **1–5**.

[figure 4(b)]. The wavelike and rope coordination modes have similar motifs. Hence, adjacent Ln(III) ions are bridged by two carboxylate groups using a  $\mu_2$ -COO<sup>−</sup> coordination mode, with Ln(III)⋯Ln(III) separations of 6.304 and 6.705 Å in **1**, 6.378 and 6.778 Å in **2**, 6.352 and 6.747 Å in **3**, 6.389 and 6.784 Å in **4**, and 6.380 and 6.773 Å in **5**.

Adjacent 1-D chains are interconnected from above and below to give a highly ordered 2-D layer coordination polymer with 16-membered rings parallel to the [1 0 0] direction [figure 5(a)]. The repeat unit in the 2-D layer grid also exhibits infinite 1-D hexagonal nano-sized cavities (approximate dimensions for Er: 0.85 × 0.99 nm) present along the [0 1 0] direction [figure 5(b)], while a butterfly-like 1-D chain is present along the [0 0 1] direction [figure 5(c)]. The coordination polymer and its topology can also be described by LOF structure shown as LnO<sub>3</sub> (O<sub>6</sub>, O<sub>8</sub>, and O<sub>5</sub>) trigonal planar (green polyhedra) joined by pyridine dicarboxylate linkers to give an extended 2-D cubic framework. The entire structure consists of an envelope of the (Ln<sub>4</sub>)O<sub>12</sub>C<sub>4</sub> clusters and pyridine dicarboxylates (PDA) as shown in figure 6(a). In each cluster, the Ln ions are arranged roughly at the vertices of a square, and the two squares are bridged by eight carboxylates, two per Ln corner [figure 6(a)]. Each Ln ion has two bridging oxygens to generate 2-D LOF, while the other four edges of Ln ions are capped by two ligands leading to the overall tetrahedral shape of the SBU [figure 6(b)]; each SBU is connected through edges ultimately responsible for construction of the 2-D net [figure 6(c)] [21, 34].

Topologically, each Ln(III) ion is a six-connected node with the Schläfli symbol of (3<sup>3</sup>·4<sup>2</sup>·5·8<sup>3</sup>·10<sup>2</sup>·11<sup>2</sup>); these connected nodes were analyzed using OLEX (figure 7) [35]. The 2-D layer coordination of **1** has a similar network as previously reported [Er<sub>2</sub>(PDA)<sub>2</sub>(*o*-bdc)(H<sub>2</sub>O)<sub>2</sub>·H<sub>2</sub>O [36]. The Er–N and Er–O bond distances are comparable to the literature values [7, 37]. The Gd–N and Gd–O bond distances of **2** are comparable to those observed in other Gd(III) complexes [37 (b) and (d), 38]. The Tb–N and Tb–O bond lengths are comparable to those reported for other Tb(III) complexes with PDA ligands [37(d), 39]. In **4**, the bond lengths of Eu–N and Eu–O are within the range of previously reported structures [10, 37(d), 39(a), 39(b), 40, 41]. The Pr–N and Pr–O bond distances of **5** are all within the range observed for other Pr(III) complexes [37(d), 39(b)]. The O–Ln–O bond angles are

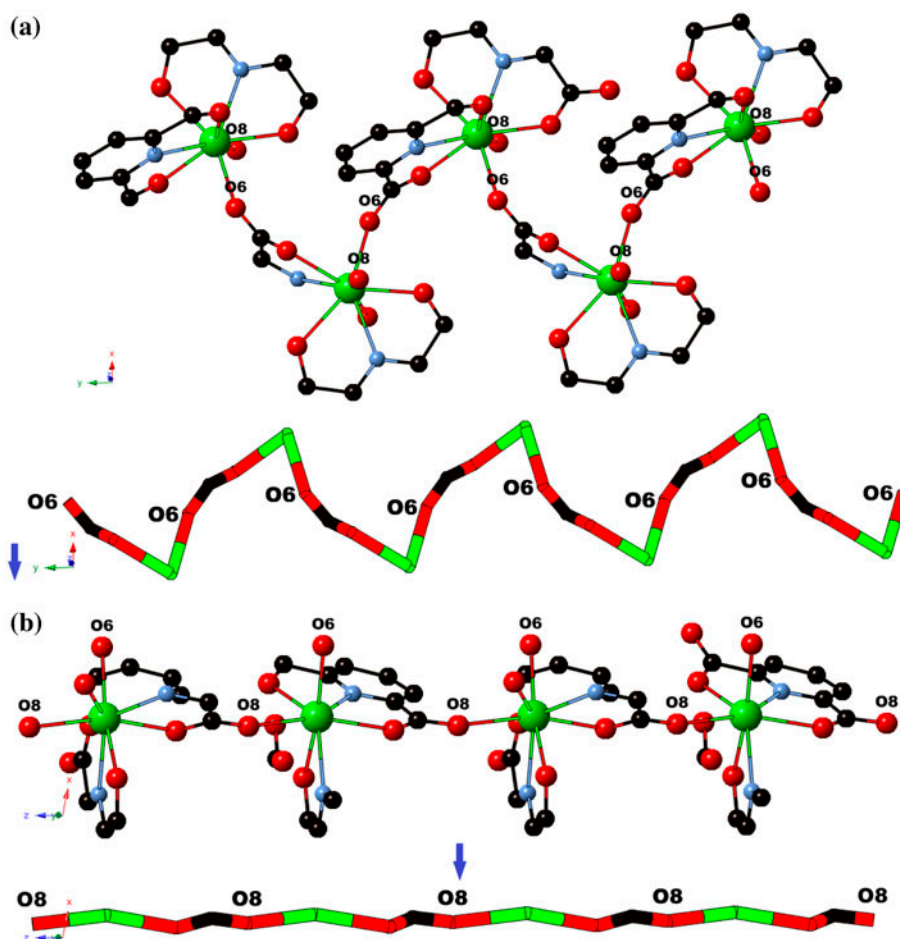


Figure 4. (a) The coordination polymer chain parallel to the [0 0 1] direction to generate wavelike 1-D polymer and (b) the coordination polymer chain parallel to the [0 1 0] direction to generate ropelike 1-D polymer in **1–5**. Ln, green; C, black; N, blue (see <http://dx.doi.org/10.1080/00958972.2015.1056739> for color version).

$76.08(10)^\circ$ – $153.41(10)^\circ$ , while the bond angles of N–Ln–O are  $62.07(16)^\circ$ – $144.45(18)^\circ$ , which are all within the range observed for other lanthanide-PDA complexes.

In **1–5**, intermolecular O–H $\cdots$ O hydrogen bonds produce a C(8) chain running parallel to the [0 1 0] direction [figure 8(a)]. Similarly, a combination of weak C–H $\cdots$ O hydrogen bonds generates a chain of edge-fused  $R_2^2(14)$  and  $R_2^2(26)$  rings running parallel to the [0 0 1] direction [figure 8(b)]. Adjacent 2-D chains of **1–5** are further extended to a 3-D hydrogen-bonded network through O–H $\cdots$ O and C–H $\cdots$ O hydrogen bonds [figure 8(b)] and  $\pi$ – $\pi$  interactions [figure 8(c)]. The C $\cdots$ O distances range from 3.110(5) to 3.373(6) Å for **1**, 3.107(8) to 3.408(8) Å for **2**, 3.106(4) to 3.403(4) Å for **3**, 3.104(5) to 3.421(5) Å for **4**, and 3.112(9) to 3.416(9) Å for **5**, respectively (table S2). LOF from **1–5** also exhibits two  $\pi$ – $\pi$  interactions between the two symmetry-related pyridine rings of neighboring molecules, with  $\pi$ – $\pi$  distances of 3.3365(17)–3.4295(17) Å for **1**, 3.386(2)–3.451(2) Å for **2**,



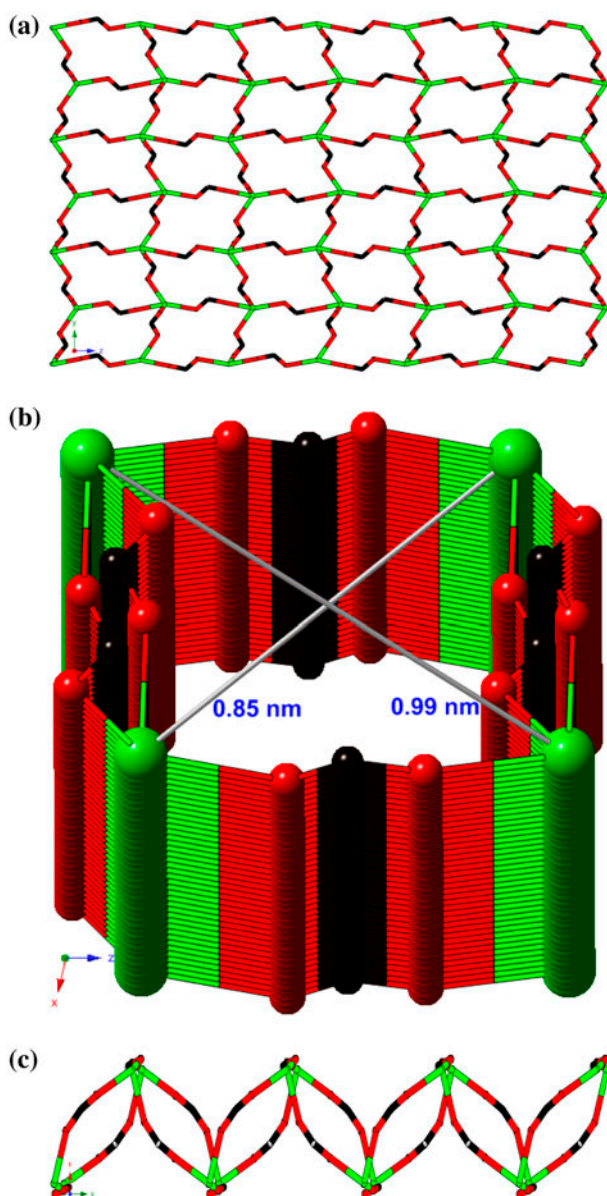


Figure 5. (a) 2-D grid motif of **1–5** constructed by interconnecting 1-D wavelike chains and ropes along the [1 0 0] direction, (b) 1-D nanosized cavities along the [0 1 0] direction, and (c) 1-D butterfly-like chain along the [0 0 1] direction.

3.3699(12)–3.4421(12) Å for **3**, 3.3962(15)–3.4622(16) Å for **4**, and 3.380(3)–3.453(3) Å for **5** (table S3).

In **1–5**, Ln–O average bond lengths decrease from 2.291 to 2.236 (Ln–O), from 2.499 to 2.442 for Ln–N, and from 9.097 to 8.561 for Ln–Ln with an increase in atomic number and can be attributed to lanthanide contraction (table 2). The abnormal behavior of bond lengths

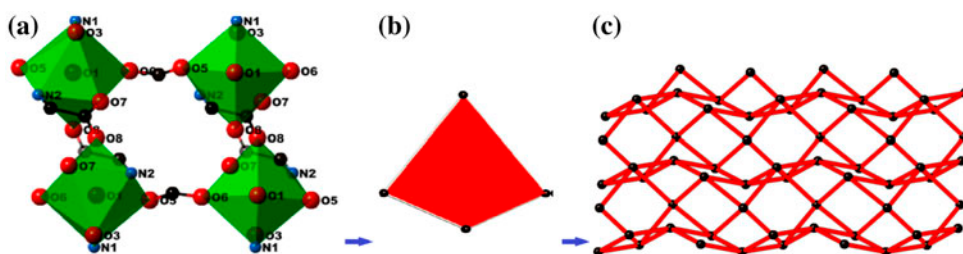


Figure 6. (a) 2-D cubic framework as the envelopes of the  $(Ln_4)O_{12}C_4$  cluster to generate tetrahedral SBU responsible for construction of 2-D net: Ln, green; C, black, (b) tetrahedra joined through carbons, and (c) 2-D coordination polymer growing through tetrahedral SBU (see <http://dx.doi.org/10.1080/00958972.2015.1056739> for color version).

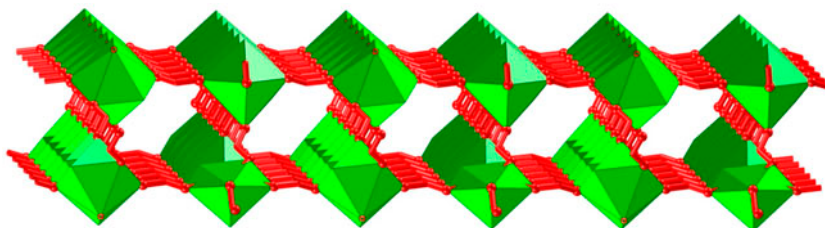


Figure 7. Schematic polyhedral view of 2-D coordination framework in 1–5.

(Ln–O and Ln–N) for the atomic radii of europium can be explained on the basis of overlapping of electron clouds. Europium tends to maintain a  $4f^7$  electron configuration and provides only two conducting electrons; thus, the overlapping of the outermost electrons between the adjacent atoms become smaller, and the atomic radius becomes larger [42].

### 3.2. Magnetic measurement

The magnetic behavior of **1**, **2**, and **3** are depicted in the forms of  $\chi_m$ ,  $\chi_m^{-1}$ , and  $\chi_m T$  versus  $T$  ( $\chi_m$  molar magnetic susceptibility) [43]. Curie–Weiss law behavior was observed above 20 K for **1** with Curie constant  $C = 12.39 \pm 0.00021 \text{ cm}^3 \text{ K mol}^{-1}$  and Weiss constant  $\theta = -8.16 \text{ K}$  (figure 9). In the high-temperature end (300 K),  $\chi_m T = 12.18 \text{ cm}^3 \text{ mol}^{-1} \text{ K}$  provides an effective magnetic moment  $\mu_{\text{eff}}$  of  $9.86 \mu_B$ , which is slightly larger than the expected value of  $9.58 \mu_B$  as per formula for one Er(III) of one uncoupled ( $g_J = 1.2$ ) ion in  $^4I_{15/2}$  ground state. The product of  $\chi_m T$  decreased with decreasing temperature to reach a final value of  $8.0 \text{ cm}^3 \text{ mol}^{-1} \text{ K}$  at 5 K with an effective magnetic moment of  $8.0 \mu_B$ .

Curie–Weiss law behavior was observed above 50 K for **2** with Curie constant  $C = 7.53 \pm 0.00123 \text{ cm}^3 \text{ K mol}^{-1}$  and Weiss constant  $\theta = -18.70 \text{ K}$  (figure S1). In the high-temperature end (300 K),  $\chi_m T = 7.28 \text{ cm}^3 \text{ mol}^{-1} \text{ K}$  provides an effective magnetic moment  $\mu_{\text{eff}}$  of  $7.63 \mu_B$ , which is slightly smaller than the expected value of  $7.94 \mu_B$  as per formula for one Gd(III) of one uncoupled ( $g_J = 2$ ) ion in  $^8S_{7/2}$  ground state. The product of  $\chi_m T$  decreased with decreasing temperature to reach a final value of  $4.42 \text{ cm}^3 \text{ mol}^{-1} \text{ K}$  at 5 K with an effective magnetic moment of  $5.95 \mu_B$ .

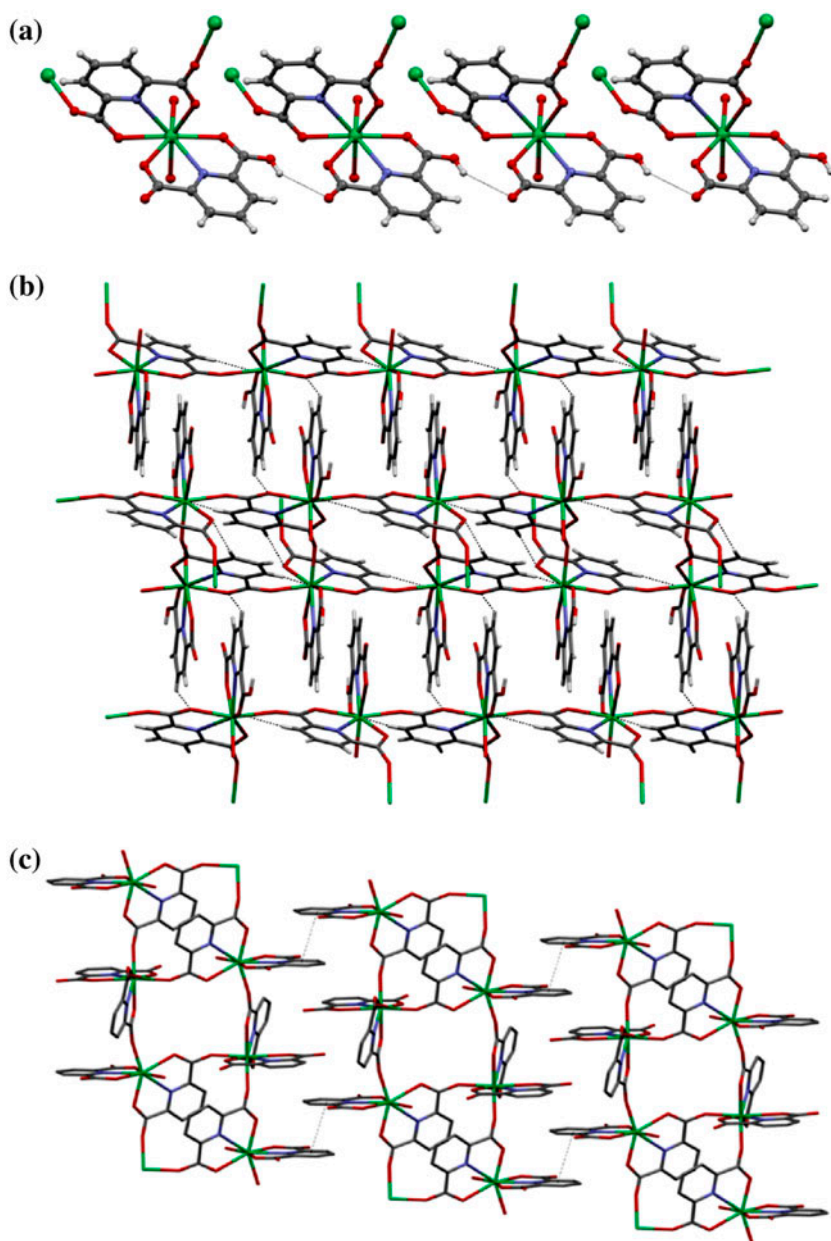
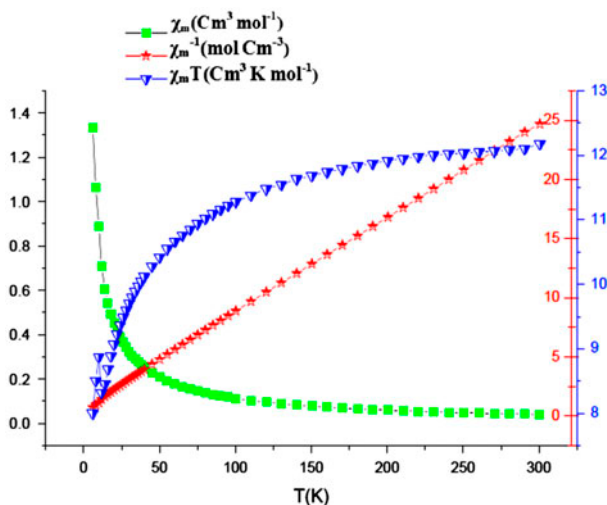


Figure 8. (a) The formation of a chain along [0 1 0] generated by O-H...O hydrogen bonds, (b) an infinite 3-D network through O-H...O and C-H...O hydrogen bonds, and (c) the  $\pi$ ... $\pi$  interactions in 1-5.

Curie-Weiss law behavior was observed above 20 K for **3** with Curie constant  $C = 12.37 \pm 0.000061 \text{ cm}^3 \text{ K mol}^{-1}$  and Weiss constant  $\theta = -2.15 \text{ K}$  (figure S2). In the high-temperature end (300 K),  $\chi_m T = 12.30 \text{ cm}^3 \text{ mol}^{-1} \text{ K}$  provides an effective magnetic moment  $\mu_{\text{eff}}$  of  $9.92 \mu_B$ , which is slightly larger than the expected value of  $9.72 \mu_B$  as per

Table 2. Bond length ranges in (Å) **1–5**.

Lanthanide	Ln–O	Ln–N
Pr	2.291(4)–2.537(4)	2.499(5)–2.505(5)
Eu	2.306(3)–2.543(3)	2.509(3)–2.526(3)
Gd	2.289(4)–2.528(4)	2.493(5)–2.512(5)
Tb	2.2781(19)–2.521(2)	2.481(2)–2.496(2)
Er	2.236(3)–2.486(3)	2.442(3)–2.459(3)

Figure 9. Temperature dependence of  $\chi_m$ ,  $\chi_m^{-1}$ , and  $\chi_m T$  for **5** at 1 KOe applied field.

formula for one Tb(III) of one uncoupled ( $g_J = 1.5$ ) ion in  ${}^7F_6$  ground state. The product of  $\chi_m T$  decreased with decreasing temperature to reach a final value of  $11.03 \text{ cm}^3 \text{ mol}^{-1} \text{ K}$  at 5 K with an effective magnetic moment of  $9.39 \mu_B$ . The overall behavior of  $\chi_m T$  with temperature and negative value of  $\theta$  for **3**, **4**, and **5** is typical for the presence of antiferromagnetic exchange coupling interactions.

### 3.3. FT-IR and thermal analyses

The decomposition pattern of **3** is illustrated in figure 10. The TGA curve passes through a flat, and the polymer starts to decompose (63.2%) beyond  $460 \text{ }^\circ\text{C}$  due to successive release of PDA accompanied by collapse of the skeleton at about  $860 \text{ }^\circ\text{C}$  (Calcd 62.6%), assuming 36.8% as the final product  $\text{Tb}_2\text{O}_3$  (Calcd 37.4%). The decomposition pattern of **4** is illustrated in figure S3. TGA curve passes through a flat, and the polymer starts to decompose (63.9%) beyond  $380 \text{ }^\circ\text{C}$  due to successive release of PDA accompanied by collapse of the skeleton up to  $780 \text{ }^\circ\text{C}$  (Calcd 63.5%), assuming 36.1% as the final product  $\text{Eu}_2\text{O}_3$  (Calcd 36.5%).

Since the complexes are very similar with same ligand, we just exemplified the FT-IR results of **1** Er(III) (figure S4) and **4** Eu(III) (figure S5), respectively. Er(III); 3364(b), 1576

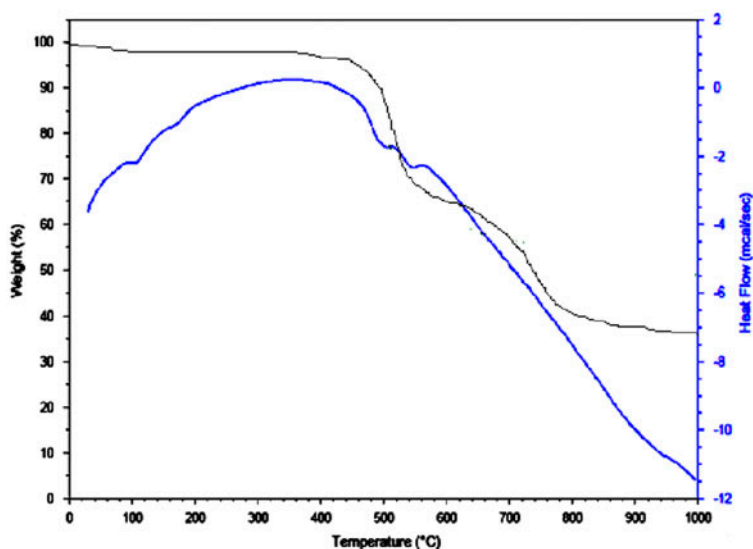


Figure 10. TGA/DSC curve of **3**, [Tb(PDA)(PDAH)]<sub>n</sub>.

(s), 1437(m), 1348(m), 1271(m), 790(m), 710(w). Eu(III); 3396(b), 1574(s), 1435(m), 1346(m), 1270(m), 789(m), 709(w). Characteristic vibrational bands are in agreement with the partially deprotonated and coordinated carboxylates [44].

#### 4. Conclusion

The isolation of five lanthanide 2-D coordination polymers based on PDAH<sub>2</sub> demonstrates that it is feasible to obtain polymeric complexes under mild hydrothermal conditions by *in situ* change in pH of the reaction mixture. This study provides an example of introducing sodium azide to increase pH of reaction mixture and ultimately deprotonation of ligand which favors thermally stable coordination networks with different degrees of dimensionality having unique topologies and fascinating properties. Further research is ongoing for better understanding of mechanism.

#### Supplementary material

CCDC reference numbers 872840 for **1**, 872841 for **2**, 872842 for **3**, 872843 for **4** and 872844 for **5** contain the supplementary crystallographic data for this study. These data can be obtained free of charge via <http://www.ccdc.cam.ac.uk/conts/retrieving.html> (or from the CCDC, 12 Union Road, Cambridge CB2 1EZ, UK; Fax: +44 1223 336 033; Email: [deposit@ccdc.cam.ac.uk](mailto:deposit@ccdc.cam.ac.uk)).

## Acknowledgments

The authors acknowledge the Higher Education Commission of Pakistan (HEC) for financing a visit to University of Oxford under IRSIP (HEC) and Dr Richard Cooper, Chemical Crystallography, Chemistry Research Laboratory, Oxford, UK, for collection of single-crystal data and magnetic measurement.

## Disclosure statement

No potential conflict of interest was reported by the authors.

## References

- [1] G. Ferey, C. Mellot-Draznieks, C. Serre, F. Millange, J. Dutour, S. Surble, I. Margiolaki. *Science*, **309**, 2040 (2005).
- [2] J.-R. Li, Y. Tao, Q. Yu, X.-H. Bu, H. Sakamoto, S. Kitagawa. *Chem. Eur. J.*, **14**, 2771 (2008).
- [3] R. Matsuda, R. Kitaura, S. Kitagawa, Y. Kubota, R.V. Belosludov, T.C. Kobayashi, H. Sakamoto, T. Chiba, M. Takata, Y. Kawazoe, Y. Mita. *Nature*, **436**, 238 (2005).
- [4] M.D. Allendorf, C.A. Bauer, R.K. Bhakta, R.J.T. Houk. *Chem. Soc. Rev.*, **38**, 1330 (2009).
- [5] Y.G. Huang, F.L. Jiang, M.C. Hong. *Coord. Chem. Rev.*, **253**, 2814 (2009).
- [6] (a) C.-J. Li, Z.-J. Lin, M.-X. Peng, J.-D. Leng, M.-M. Yang, M.-L. Tong. *Chem. Commun.*, **47**, 6348 (2008); (b) X.H. Li, Y.P. Wang, Z.Y. Ma, R.L. Zhang, J.S. Zhao. *J. Coord. Chem.*, **63**, 1029 (2010).
- [7] H.-S. Wang, B. Zhao, B. Zhai, W. Shi, P. Cheng, D.-Z. Liao, S.-P. Yan. *Cryst. Growth Des.*, **7**, 1851 (2007).
- [8] B. Zhao, P. Cheng, Y. Dai, C. Cheng, D.-Z. Liao, S.-P. Yan, Z.-H. Jiang, G.-L. Wang. *Angew. Chem. Int. Ed.*, **42**, 934 (2003).
- [9] T.K. Prasad, M.V. Rajasekharan. *Inorg. Chem.*, **48**, 11543 (2009).
- [10] (a) J. Hamacek, S. Zebret, G. Bernardinelli. *Polyhedron*, **28**, 2179 (2009); (b) H.-S. Wang, G.-C. Li, Y. Chen, Z.-J. Zhang, M.-L. Liu. *J. Coord. Chem.*, **63**, 4068 (2010); (c) L.-Z. Chen, F.-M. Wang, H. Shu. *J. Coord. Chem.*, **65**, 439 (2012).
- [11] J. Lu, T. Paliwala, S.C. Lim, C. Yu, T. Niu, A. Jacobson. *J. Inorg. Chem.*, **36**, 923 (1997).
- [12] M. Munakata, G.L. Ning, T. Kuroda-Sowa, M. Maekawa, Y. Suenaga, T. Horino. *Inorg. Chem.*, **37**, 5651 (1998).
- [13] O.S. Jung, S.H. Park, K.M. Kim, H.G. Jang. *Inorg. Chem.*, **37**, 5781 (1998).
- [14] P. Losier, M.J. Zaworotko. *Angew. Chem. Int. Ed. Engl.*, **35**, 2779 (1996).
- [15] K. Li, H. Jiang, G. Lian, Q. Wang, X. Zhao, D. Cui, X. Tao. *Chin. Sci. Bull.*, **52**, 1785 (2007).
- [16] R.W. Gable, B.F. Hoskins, R. Robson. *J. Chem. Soc., Chem. Commun.*, 1677 (1990).
- [17] M. Fujita, Y.J. Kwon, S. Washizu, K. Ogura. *J. Am. Chem. Soc.*, **116**, 1151 (1994).
- [18] S.C. Manna, J. Ribas, E. Zangrando, N. Ray Chaudhuri. *Inorg. Chim. Acta*, **360**, 2589 (2007).
- [19] (a) B. Zhao, L. Yi, Y. Dai, X.Y. Chen, P. Cheng, D.Z. Liao, S.P. Yan, Z.H. Jiang. *Inorg. Chem.*, **44**, 911 (2005); (b) Y.L. Lu, J.Y. Wu, M.C. Chan, S.M. Huang, C.S. Lin, T.W. Chiu, Y.H. Liu, Y.S. Wen, C.H. Ueng, T.M. Chin, C.H. Hung, K.L. Lu. *Inorg. Chem.*, **45**, 2430 (2006); (c) S. Sharif, O. Sahin, I.U. Khan, O. Büyükgüngör. *J. Coord. Chem.*, **65**, 1892 (2012); (d) S. Sharif, I.U. Khan, S. Zaheer, S.W. Ng. *Acta Crystallogr.*, **E68**, m624 (2012); (e) I.U. Khan, S. Sharif, O. Sahin. *J. Coord. Chem.*, **66**, 3113 (2013); (f) S. Sharif, O. Sahin, I.U. Khan, O. Büyükgüngör, W.T.A. Harrison. *Crystals*, **3**, 1253 (2012); (g) S. Sharif, I.U. Khan, O. Sahin, S. Ahmad, O. Büyükgüngör, S. Ali. *J. Inorg. Organomet. Polym.*, **22**, 1165 (2012).
- [20] (a) Y. Zhang, W. Ju, X. Xu, Y. Lv, D. Zhu, Y. Xu. *Crystallogr. Eng. Commun.*, **16**, 5681 (2014); (b) Y. Chang, Z. Pei, Q. Shuai. *J. Coord. Chem.*, **66**, 3137 (2013); (c) Y. Chen, Q. Gao, D. Gao, D. Wang, Y. Li, W. Liu, W. Li. *J. Coord. Chem.*, **66**, 3829 (2013); (d) X. Li, Q.Y. Lian, Q.H. Meng, Y.F. Luo, R.H. Zenga. *Acta Crystallogr.*, **E65**, m1288 (2009); (e) K. Huang, C. Hu. *J. Coord. Chem.*, **61**, 472 (2008); (f) Y.Q. Sun, J. He, Z.T. Xu, G. Huang, X.P. Zhou, M. Zeller, A.D. Hunter. *Chem. Commun.*, **45**, 4779 (2007); (g) K.H. Li, Z.T. Xu, H.H. Xu, P.J. Carroll, J.C. Fettinger. *Inorg. Chem.*, **45**, 1032 (2006); (h) A. Fernandes, J. Jaud, J.D. Ghys, C.B. Cabarrecq. *Polyhedron*, **20**, 2385 (2001).
- [21] D.J. Tranchemontagne, J.L. Mendoza-Cortés, M. O'Keeffe, O.M. Yaghi. *Chem. Soc. Rev.*, **38**, 1257 (2009).
- [22] Nonius. *COLLECT*, Nonius BV, Delft (2001).
- [23] Z. Otwinowski, W. Minor. In *Methods in Enzymology*, *V*, 276, *Macromolecular Crystallography; Part A*, C.W.J. Carter, R.M. Sweet (Ed.), Academic Press, New York (1997).

- [24] G.M. Sheldrick. *Acta Crystallogr., Sect. A: Found. Crystallogr.*, **64**, 112 (2008).
- [25] P.W. Betteridge, J.R. Carruthers, R.I. Cooper, K. Prout, D.J. Watkin. *J. Appl. Crystallogr.*, **36**, 1487 (2003).
- [26] A.L. Spek. *J. Appl. Crystallogr.*, **36**, 7 (2003).
- [27] C.F. Macrae, I.J. Bruno, J.A. Chisholm, P.R. Edgington, P. McCabe, E. Pidcock, L. Rodriguez-Monge, R. Taylor, J. Van de Streek, P.A. Wood. *J. Appl. Crystallogr.*, **41**, 466 (2008).
- [28] L.J. Farrugia. *J. Appl. Crystallogr.*, **32**, 837 (1999).
- [29] *Crystal and Molecular Structures Programme for Mac and Windows*. CrystalMaker® Software, Ltd, Oxford. Available online at: [www.crystallmaker.com](http://www.crystallmaker.com).
- [30] M.C. Das, S.K. Ghosh, E.C. Sanudo, P.K. Bharadwaj. *Dalton Trans.*, **9**, 1644 (2009).
- [31] C.-J. Li, W. Li, Z.-S. Meng, M.-X. Peng, M.-M. Yang, M.-L. Tong. *Aust. J. Chem.*, **62**, 1607 (2009).
- [32] *OriginPro 8 SRO, V 8.0724 (B724)*, Northampton, MA 01060, USA. Available online at: [www.originlab.com](http://www.originlab.com).
- [33] (a) P.W. Selwood. *Magnetochemistry*, Interscience Publishers, New York (1956); (b) S. Blundell, D. Thouless. *Magnetism in Condensed Matter*, Oxford University Press, Oxford (2001); (c) B. Want, F. Ahmad, P.N. Kotru. *J. Alloys Compd.*, **448**, L5 (2008).
- [34] O.M. Yaghi, M. O'Keeffe, N.W. Ockwig, H.K. Chae, M. Eddaoudi, J. Kim. *Nature*, **423**, 705 (2003).
- [35] O.V. Dolomanov, A.J. Blake, N.R. Champness, M. Schröder. *J. Appl. Crystallogr.*, **36**, 1283 (2003).
- [36] W.Z. Longa, Z.S. Tian, Y.G. Yu. *Chin. J. Struct. Chem.*, **29**, 17 (2010).
- [37] (a) C.X. Cheng, H.W. Liu, Z.Q. Hu, F.H. Luo, M.N. Cao. *Acta Crystallogr.*, **E63**, m1 (2007); (b) H.L. Gao, L. Yi, B. Zhao, X.Q. Zhao, P. Cheng, D.Z. Liao, S.P. Yan. *Inorg. Chem.*, **45**, 5980 (2006); (c) P.A. Brayshaw, A.K. Hall, W.T.A. Harrison, J.M. Harrowfield, D. Pearce, T.M. Shand, B.W. Skelton, C.R. Whitaker, A.H. White. *Eur. J. Inorg. Chem.*, 1127 (2005); (d) Q.B. Bo, G.X. Sun, D.L. Geng. *Inorg. Chem.*, **49**, 561 (2010); (e) D.Y. Ma, W.X. Wang, Y.W. Li. *J. Coord. Chem.*, **63**, 448 (2010).
- [38] (a) A.K. Hall, J.M. Harrowfield, B.W. Skelton, A.H. White. *Acta Crystallogr.*, **C56**, 407 (2000); (b) L.J. Hao, T.L. Yu. *Acta Crystallogr.*, **E63**, m1967 (2007); (c) T. Zhu, K. Ikarashi, T. Ishigaki, K. Uematsu, K. Toda, H. Okawa, M. Sato. *Inorg. Chim. Acta*, **362**, 3407 (2009); (d) X.D. Yang, C.H. Zhang, D.P. Wang, Y.G. Chen. *Inorg. Chem. Commun.*, **13**, 1350 (2010).
- [39] (a) M.S. Liu, Q.Y. Yu, Y.P. Cai, C.Y. Su, X.M. Lin, X.X. Zhou, J.W. Cai. *Cryst. Growth Des.*, **8**, 4083 (2008); (b) X.Q. Zhao, Y. Zuo, D.L. Gao, B. Zhao, W. Shi, P. Cheng. *Cryst. Growth Des.*, **9**, 3948 (2009); (c) L. Chen, X.H. Yin, M.Y. Tan, C.G. Xia, K.B. Yu. *Acta Crystallogr.*, **E58**, m666 (2002).
- [40] (a) J. Xu, W. Su, M. Hong. *Cryst. Growth Des.*, **11**, 337 (2011); (b) C.B. Cabarrecq, J.C. Trombe. *J. Chem. Crystallogr.*, **39**, 786 (2009).
- [41] X. Liu, Y. Jia, Y. Zhang, R. Huang. *Eur. J. Inorg. Chem.*, 4027 (2010).
- [42] C. Huang. *Rare Earth Coordination Chemistry Fundamentals and Applications*, Chap. 1, pp. 4–6, John Wiley & Sons, Singapore (2010).
- [43] (a) A.F. Orchard. *Magnetochemistry*, Oxford University Press, Oxford (2003); (b) C. Kittel. *Introduction to Solid State Physics*, 2nd Edn, J. Wiley and Sons, New York (1953); (c) R.L. Carlin. *Magnetochemistry*, Springer-Verlag, Berlin (1986); (d) O. Kahn. *Molecular Magnetism*, VCH Publishers Inc, New York (1993).
- [44] (a) P. Carmona. *Spectrochim. Acta*, **36**, 705 (1980); (b) K. Nakamoto. *Infrared Spectra of Inorganic and Coordination Compounds*, Wiley Interscience, New York (1963); (c) X. Xu, X. Liu, T. Sun, X. Zhang, E. Wang. *J. Coord. Chem.*, **62**, 2775 (2009); (d) J. Yi, Z. Fu, S. Liao. *J. Coord. Chem.*, **62**, 2290 (2009).